Bull. Astr. Soc. India (1999) **27**, 567-582

Infrared diagnostics for compact H II Regions - I

Bhaswati Mookerjea[1] and S. K. Ghosh[2]

Tata Institute of Fundamental Research, Homi Bhabha Road, Mumbai 400005, India

Received 25 April 1999; accepted 16 July 1999

Abstract. Compact H II regions have been modelled realistically covering multidimensional parameter space in an effort to develop diagnostic tools. These models consist of embedded exciting ZAMS stars with a spherical cloud of dust and gas around them. Three types of embedded stars are considered, viz., O4, O7 and B0.5. Different radial density distribution laws (r^0 and r^{-1}) and total radial optical depths have been considered. These models are further constrained by the total gas and dust mass (possibly available from CO observations) of the cloud.

Radiation transfer calculations through the gas and the dust components have been carried out to predict the emergent spectral energy distribution (SED) and directly observables like : infrared photometric colours, angular sizes and radio continuum emission. Many of these predictions have been quantified in such a way that, they can be directly compared with the data from the instruments onboard the Infrared Space Observatory (ISO).

In general mid-IR photometric data are found to be diagnostically much more powerful compared to the far-IR measurements. The capability of different far and mid infrared colours to extract information about the embedded stellar type, radial density distribution, and the total optical depth have been demonstrated.

The present work has been followed up with another study, in which, the constraints on the interstellar cloud are more relaxed. Additionally, the gas component has been considered in much greater details so as to include predictions about fine structure line emission of several heavy elements (Mookerjea & Ghosh, 1999, Paper II), observable using ISO.

Key words : compact H II regions - radiative transfer - infrared colours

[1]bhaswati@tifr.res.in, [2]swarna@tifr.res.in

1. Introduction

The formation and the initial stages of evolution of stars take place inside dense regions within molecular clouds, from which they are born. Hence, the star formation studies have necessarily to deal with the protostars / young stars in the environment of interstellar gas and dust of the parent cloud. The stars with sufficient supply of Lyman continuum photons (basically depending on their mass) create and maintain H II regions around them. The (ultra)/compact variety of H II regions in particular provides a natural test case for better understanding of medium to high mass star formation. They present two main advantages for such studies : being younger they allow one to probe the physical processes closer in time to the formation of the embedded star, and secondly they usually have simpler geometrical shapes (e.g. with spherical / cylindrical symmetry), thus providing opportunity of direct comparison with the predictions of detailed numerical models. In addition, since they belong to higher luminosity class, (between ZAMS O4 to B0.5), they can be studied observationally over larger distances (almost any part of the Galaxy) in the radio continuum as well as infrared / sub-mm.

In this study we have considered models of compact H II regions, each consisting of a spherically symmetric envelope of gas and dust, immersed in an isotropic interstellar radiation field (ISRF), with an embedded ZAMS star as the central source of energy. The radiation transfer calculations through the gas and the dust have been carried out self-consistently. Effects of (i) different types of ZAMS stars as central exciting sources, (ii) various radial density distributions (of the gas and the dust), and (iii) the radial optical depth, on the continuum emission from both the dust and the gas components have been studied. These models predict the dust continuum emission over a wide spectral region covering right from the UV to the

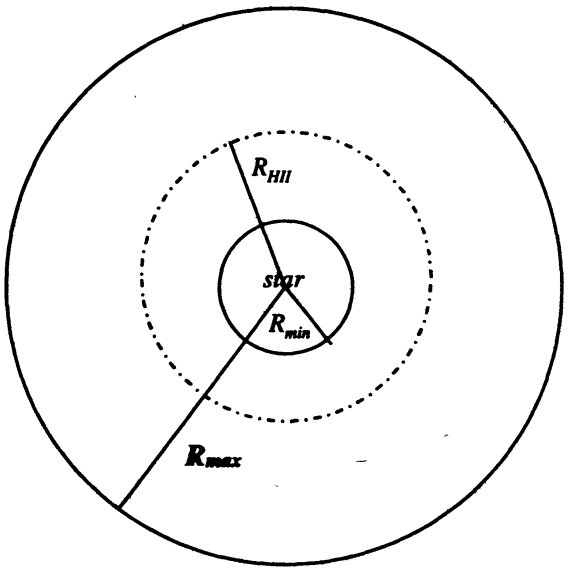

Figure 1. Schematic diagram of the spherical compact H II region surrounded by a dusty molecular cloud. The region with $r \leq R_{min}$ consists of only gas, ionized and/or neutral, the region between R_{min} and R_{HII} contains ionized gas and dust and the region between R_{HII} and R_{max} contains neutral gas and dust (if $R_{HII} > R_{min}$; as in the figure). In general R_{HII} could also be $< R_{min}$.

millimetre wavelengths; and the radio continuum emission from the gas, at any selected frequency (5 GHz in the present study). For the sake of easy comparability, these predictions have been presented in terms of quantities that can be observed by the various relevant instruments onboard the Infrared Space Observatory (ISO, the most sophisticated infrared space mission to date; Kessler et al. (1996)). These quantities have been presented in the form of expected (i) colours between various ISOPHOT filters, (ii) radial profiles / half power sizes in various ISOCAM filter pass bands, and (iii) the ratio of radio continuum to far infrared emission.

2. Modelling the compact H II regions

Detailed numerical modelling involving radiative transfer with realistic assumptions needs to be performed, in order to achieve similar (or even better) accuracy in predicting (i) the emergent continuum and line spectrum, and (ii) the structural details as a function of wavelength, as expected from instruments onboard ISO.

With the above aim in mind, a simple model, considering a compact H II region as a spherically symmetric cloud (made of typical interstellar gas-dust material), powered by a centrally embedded zero age main sequence star, is considered. This cloud is assumed to be immersed in an isotropic radiation field (typical Interstellar Radiation Field, ISRF). The interstellar gas and the dust is assumed to follow the same radial density distribution law, but with the following difference - whereas the gas exists throughout the cloud (i.e. right from the stellar surface upto the outer boundary of the cloud, R_{max}; see Figure 1), there is a natural lower limit to the inner boundary, R_{min}, for the dust distribution (i.e. a cavity in the dust cloud). This is because the dust grains are destroyed when exposed to excessive radiative heating. The gas to dust ratio, where they co-exist ($R_{min} < r < R_{max}$), is assumed to be constant. As a simplistic approach, the interstellar gas is assumed to be consisting of hydrogen only. The position of the ionization front (R_{HII}, refer to Figure 1) depends on the effective temperature and luminosity of the exciting star, as well as the gas density. The case, $R_{HII} < R_{min}$ is also possible, if either the star is not hot enough and / or the gas density in the vicinity of the star is quite high. The gas component is assumed to have a uniform elemental abundance throughout the cloud, though the ionization structure and the various level populations depend on several physical parameters including the local radiation field.

Families of models have been constructed to cover three primary parameters, viz., (1) the radial density distribution; (2) the spectral type of the embedded ZAMS star (determining the luminosity and the shape of the input spectrum); and (3) the total radial optical depth at a fiducial wavelength. All other relevant variables are either determined self-consistently by the primary parameters or chosen to be fixed at some reasonable values.

This modelling scheme involves the use of a modified version of the code CSDUST3 (Egan et al., 1988). This code takes into account the effects of multiple scattering, absorption and re-emission on the temperature of dust grains and the internal radiation field. In addition, the radiation field anisotropy, linear anisotropic scattering and multigrain components are also considered. This code has been modified by us and the main modification has been in terms of incorporating gas and dust self-consistently, in order to calculate emission from both. More details of this modification are presented in Mookerjea & Ghosh (1999) and also in Appendix

Table 1. Details of the central stars used for this study.

Spectral type	Luminosity	T_{eff}	N_{Lyc}
	$L_\odot$	K	Sec^{-1}
O4	1.260×10^6	50000	5.811×10^{49}
O7	1.000×10^5	38500	3.630×10^{48}
B0.5	1.064×10^4	26200	1.318×10^{46}

A. This scheme considers photo-ionization and recombination, along with absorption due to the grains. Self-absorption of the radio emission within the cloud has also been considered in this scheme, but the gas-dust coupling has been neglected. Details about the considerations regarding energetic of this scheme have been presented in Mookerjea et al. (1999). Additional numerical details about the code are presented in Appendix B.

2.1 The dust component

The physical properties and the size distribution of the interstellar dust grains have been fixed to a very widely accepted variety for all our models. An equal mixture (50% : 50%) of Graphite and Astronomical Silicate grains, and a gas to dust ratio of 100 : 1 by mass, have been considered. All physical properties of the grains, viz., absorption, scattering efficiencies and linear anisotropy factor have been taken from Draine & Lee (1984) and Laor & Draine (1993). Averaging over 29 discrete sizes have been performed, following a size distribution of $n(a)da \sim a^{-m}da$, $a_{min} \leq a \leq a_{max}$ with m = 3.5 (Mathis et al., 1977). The lower and upper limits of the grain size distribuion, a_{min} (0.01 μm) and a_{max} (0.25 μm), have been taken from Mathis et al. (1983).

2.2 The Models

The constraints on the family of models presented here are such that they are useful to explain emissions from compact H II regions, for which both total luminosity and mass (gas+dust) are available from observations. All models are constrained by a total mass, M_T of 2.7×10^4 $M_\odot$ and the luminosity is constrained by the type of ZAMS star embedded at the centre. The outer boundary condition is provided by the ISRF taken from Mathis et al., (1983). Three types of ZAMS stars, viz., O4, O7 and B0.5, with luminosity covering a range of two orders of magnitude, are considered. The stellar type also determines the flux of photons with $\lambda < 912$ Å and hence has a direct bearing on the radio continuum calculations. In this study, stellar parameters like luminosity, effective temperature and number of Lyman continuum photons emitted per sec, have been taken from Thompson (1984) and the stellar luminosity for $\lambda < 912$ Å has been obtained from Panagia (1973). The stellar characteristics used here, are presented in Table 1. For each stellar type, both r^0 and r^{-1} density distributions are considered. Again, for each density distribution, a family of 12 models with the total radial optical depth (defined at the wavelength of 100 μm, hereafter τ_{100}) ranging from 0.005 to 0.260 are considered. The r^{-2} density distribution has not been considered here, since for the M_T and range of τ_{100} explored, the cloud sizes become too large and unphysical.

The geometrical details of the models are determined as follows : R_{min} is determined by the sublimation temperature of dust and the stellar luminosity, hence it remains the same for a particular stellar type; R_{max} for each model is determined from the total mass, τ_{100}, and the radial density distribution; the extent of the H II region (R_{HII}) is determined by the embedded

Table 2. Parameters for models with O4 as exciting star.

τ_{100}	r^0				r^{-1}			
	R_{min}	R_{max}	R_{HII}	$n_d(R_{min})$	R_{min}	R_{max}	R_{HII}	$n_d(R_{min})$
	(10^{-4}pc)	(pc)	(10^{-2}pc)	(10^{-7}cm^{-3})	(10^{-4}pc)	(pc)	(10^{-3}pc)	(10^{-4}cm^{-3})
0.005	2.10	14.21	341	0.122	2.40	35.99	410	0.752
0.0075	2.10	11.60	209	0.224	2.40	29.05	108	1.153
0.010	2.20	10.05	148	0.345	2.40	24.96	48.1	1.563
0.015	2.20	8.20	89.6	0.635	2.40	20.14	19.0	2.399
0.020	2.20	7.10	62.7	0.977	2.40	17.29	11.4	3.254
0.040	2.30	5.02	26.3	2.765	2.20	12.04	4.71	7.328
0.060	2.30	4.10	15.7	5.080	2.10	9.73	3.42	11.74
0.080	2.30	3.55	10.9	7.822	2.00	8.38	2.85	16.64
0.100	2.30	3.18	8.22	10.93	1.80	7.49	2.38	23.13
0.150	2.30	2.59	4.92	20.09	1.70	6.06	2.02	37.43
0.200	2.40	2.25	3.44	30.94	1.50	5.24	1.70	56.69
0.260	2.40	1.97	2.49	45.87	1.30	4.60	1.43	84.91

Table 3. Parameters for models with O7 as exciting star.

τ_{100}	r^0				r^{-1}			
	R_{min}	R_{max}	R_{HII}	$n_d(R_{min})$	R_{min}	R_{max}	R_{HII}	$n_d(R_{min})$
	(10^{-4}pc)	(pc)	(10^{-2}pc)	(10^{-7}cm^{-3})	(10^{-4}pc)	(pc)	(10^{-4}pc)	(10^{-4}cm^{-3})
0.005	5.00	14.21	165	0.122	6.20	38.56	654	0.268
0.0075	5.40	11.60	105	0.224	6.20	31.18	198	0.411
0.010	5.40	10.05	75.7	0.345	6.20	26.81	95.2	0.564
0.015	5.60	8.20	47.5	0.635	6.20	21.67	40.9	0.877
0.020	5.60	7.11	34.0	0.977	6.20	18.63	25.6	1.226
0.040	5.80	5.02	15.0	2.763	5.80	12.99	11.5	2.772
0.060	5.80	4.10	9.22	5.077	5.60	10.51	8.61	4.583
0.080	5.80	3.55	6.50	7.817	5.20	9.07	7.10	6.743
0.100	5.80	3.18	4.96	10.92	4.80	8.10	6.11	9.128
0.150	5.80	2.59	3.01	20.07	4.40	6.57	5.09	16.31
0.200	5.90	2.25	2.12	30.90	3.80	5.69	4.21	24.88
0.260	5.90	1.97	1.53	45.81	3.50	4.98	3.75	36.30

stellar type and the radial density profiles of the interstellar material of the cloud. All these parameters are presented in Tables 2, 3 and 4 for embedded stellar types O4, O7 and B0.5 respectively.

Table 4. Parameters for models with B0.5 as exciting star.

τ_{100}	r^0				r^{-1}			
	R_{min} (10^{-4}pc)	R_{max} (pc)	R_{HII} (10^{-3}pc)	$n_d(R_{min})$ ($10^{-7}cm^{-3}$)	R_{min} (10^{-4}pc)	R_{max} (pc)	R_{HII} (10^{-6}pc)	$n_d(R_{min})$ ($10^{-4}cm^{-3}$)
0.005	1.40	14.21	323	0.122	1.80	40.75	2320	0.781
0.0075	1.40	11.60	213	0.224	1.80	32.99	1070	1.192
0.010	1.40	10.05	158	0.345	1.80	28.39	675	1.609
0.015	1.40	8.20	104	0.635	1.80	22.97	405	2.457
0.020	1.50	7.11	76.7	0.977	1.80	19.77	305	3.319
0.040	1.50	5.02	36.8	2.763	1.70	13.79	132	7.217
0.060	1.50	4.10	23.9	5.076	1.60	11.19	57.0	11.66
0.080	1.50	3.55	17.5	7.815	1.50	9.65	31.6	16.70
0.100	1.50	3.18	13.8	10.92	1.50	8.59	19.8	21.10
0.150	1.60	2.59	8.85	20.07	1.30	6.99	8.69	36.73
0.200	1.60	2.25	6.45	30.89	1.20	6.04	4.83	53.38
0.260	1.60	1.97	4.82	45.79	1.10	5.28	2.83	76.03

3. Results

3.1 Continuum spectral energy distribution

The emergent continuum Spectral Energy Distribution (SED) from each model, as resulting from the radiation transfer calculations through the dust component have been translated into directly measurable quantities keeping in mind the photometer ISOPHOT (Lemke et al., 1996) onboard the space mission, ISO. This photometer covers wavebands between 2.5 and 240 μm, and hence is well suited to sample the entire infrared SED. A set of ISOPHOT filters have been carefully selected for this purpose, which represent the continuum SED originating from the dust grains in thermal equilibrium (e.g. avoiding filters specially planned for features due to the non-equilibrium processes of Polycyclic Aromatic Hydrocarbon (PAH) or Very Small Grains (VSG) etc; Puget & Leger, 1989). The predicted spectrum has been convolved with the ISOPHOT filter responses (as a function of wavelength; Klaas et al., 1994) to calculate the expected signals. A list of these filters and their respective specifications are presented in Table 5. In all, five PHT-P filters and three PHT-C filters have been chosen to cover the entire mid to far infrared region. The predicted colours between the selected PHT-P and PHT-C bands, are presented as a function of τ_{100} in Figures 2 - 4 for the families of models explored here. Throughout the present paper, by "colour", we refer to the logarithm (to the base of 10) of the

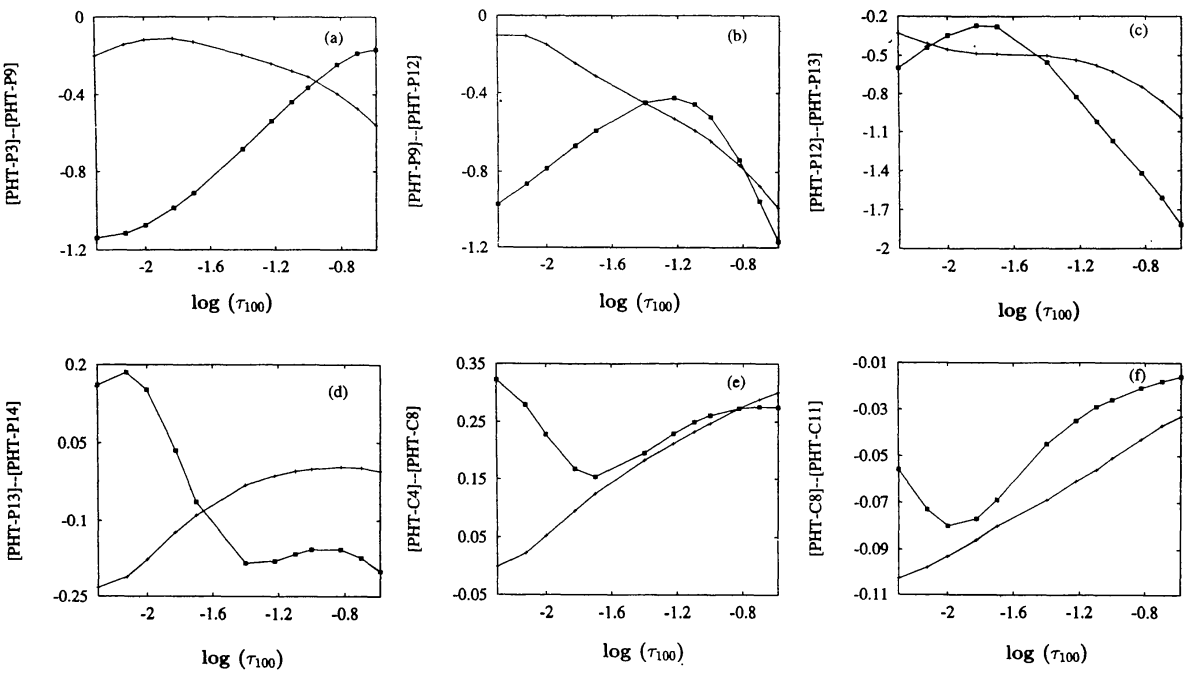

Figure 2. Plots of colours as a function of optical depth τ_{100}, for an exciting star of type O4. The symbols □ and + represent r^0 and r^{-1} density distributions respectively. The ordinates of the plots are : Colour using PHT-P3 and PHT-P9 filters in (a), PHT-P9 and PHT-P12 filters in (b), PHT-P12 and PHT-P13 filters in (c), PHT-P13 and PHT-P14 filters in (d), PHT-C4 and PHT-C8 filters in (e), PHT-C8 and PHT-C11 filters in (f).

ratio of flux densities. The colours have been selected such that (i) both the filters defining a particular colour correspond to the same sub-instrument (e.g. either PHT-P or PHT-C); and (ii) the colours represent local slopes of the SEDs (i.e. using filters neighbouring in effective wavelength). Figures 2, 3 and 4 represent the variation of colours as a function of τ_{100} corresponding to a central star of type O4, O7 and B0.5 respectively. Only those colours which are sensitive to τ_{100} and hence have important diagnostic value, have been presented here. In each figure, two sets of model predictions are presented corresponding to the dust density distribution laws proportional to r^0 and r^{-1} (with all other constraints being identical).

The results of the radiative transfer of Lyman continuum photons through the gas (pure hydrogen) and the dust where it co-exists, as described in Appendix-A, are presented in terms of ratio of radio to far-IR emission. In Figure 5 the ratio of the predicted flux densities at 5 GHz and 60 μm are displayed as a function of τ_{100}. Once again different curves correspond to different density distribution laws as explained in their captions.

3.2 Spatial / structural information

Next, the diagnostic power of spatial / structural information has been assessed quantitatively. The structural information of the gas+dust cloud models considered here consist of spatial variation of intensity across the source at different wavelengths. Since all models are spherically symmetric, the structural information is basically one dimensional. In order to concisely present

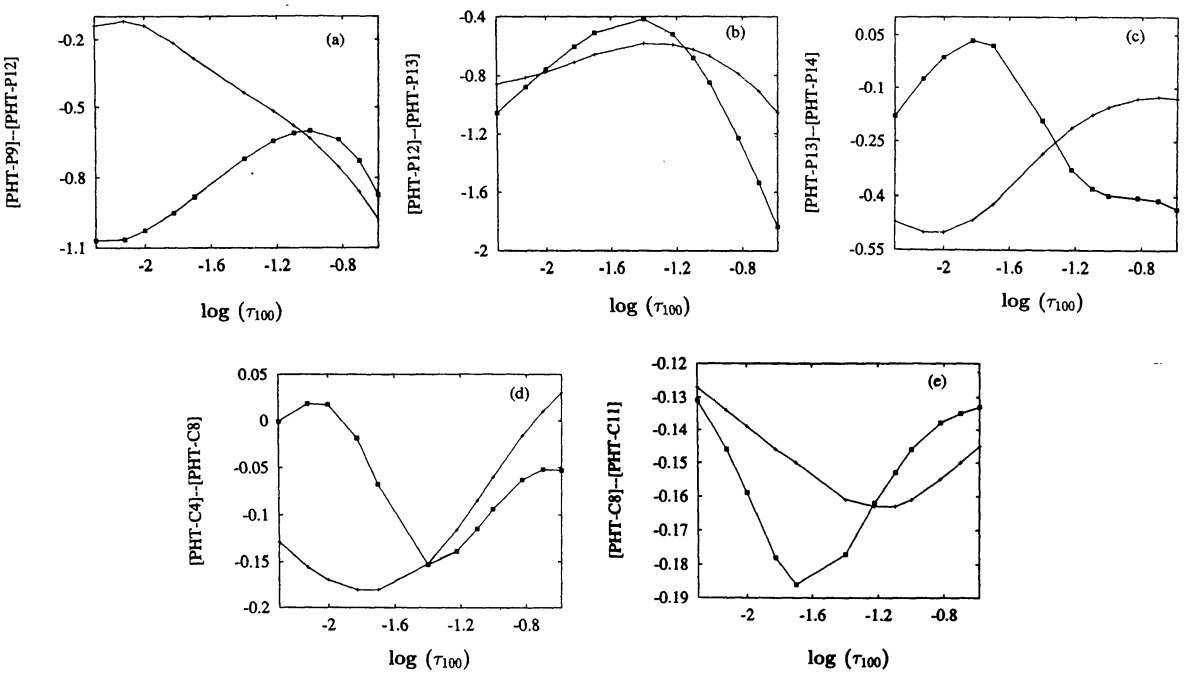

Figure 3. Plots of colours as a function of optical depth, τ_{100} for an exciting star of type O7. The symbols □ and + represent r^0 and r^{-1} density distributions respectively. The ordinates of the plots are : Colour using PHT-P9 and PHT-P12 filters in (a), PHT-P12 and PHT-P13 filters in (b), PHT-P13 and PHT-P14 filters in (c), PHT-C4 and PHT-C8 filters in (d), PHT-C8 and PHT-C11 filters in (e).

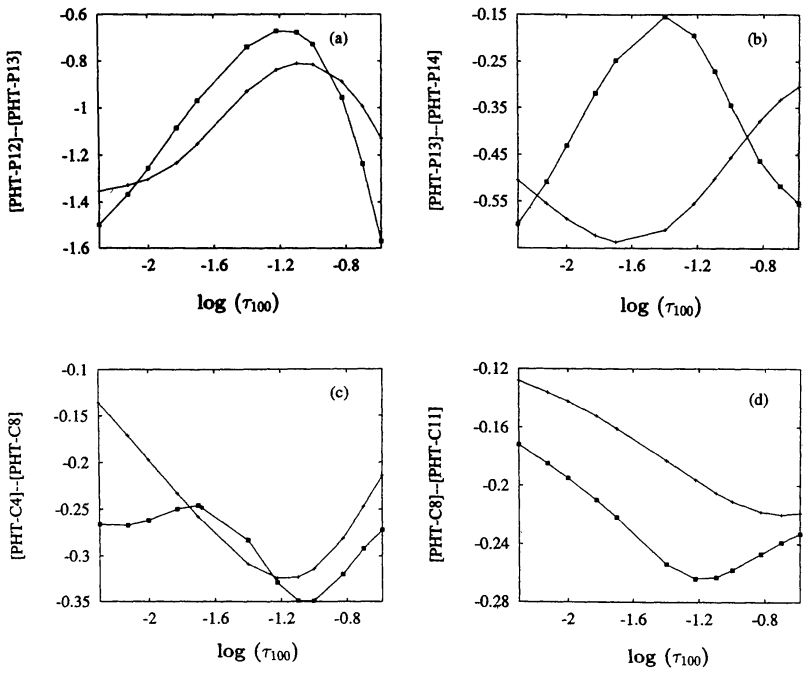

Figure 4. Plots of colours as a function of optical depth, τ_{100} for an exciting star of type B0.5. The symbols □ and + represent r^0 and r^{-1} density distributions respectively. The ordinates of the plots are : Colour using PHT-P12 and PHT-P13 filters in (a), PHT-P13 and PHT-P14 filters in (b), PHT-C4 and PHT-C8 filters in (c), PHT-C8 and PHT-C11 filters int (d).

Table 5. Details of ISOPHOT (PHT) & ISOCAM (CAM) filters chosen.

Instrument	Filter #	λ_{centre}	$\Delta\lambda$
		μm	μm
PHT-P	3	4.86	1.55
	9	12.83	2.33
	12	23.81	9.18
	13	60.06	25.48
	14	101.63	40.15
PHT-C	4	95.1	51.4
	8	161.0	82.5
	11	204.6	67.3
CAM-SW	3	4.50	1.00
	4	2.77	0.55
	9	3.88	0.24
CAM-LW	5	6.75	0.50
	8	11.4	1.30
	9	15.0	2.00

these information, the half width at half maximum (HWHM) as a function of wavelength, has been considered to be the primary parameter. The imaging instrument onboard ISO, the ISOCAM, is well suited for studying structural details in the wavelength range 2.5 to 18 mm. This instrument images regions of ~ 3′ × 3′ with an angular resolution of ~ 6″ in various filters (CAM-SW covers 2.5 to 5.5 mm; CAM-LW covers 4 to 18 mm; Cesarsky et al., 1996). Three bands each of CAM-SW as well as CAM-LW have been selected (see Table 5) for predicting HWHM sizes at their corresponding central wavelengths. In order to get an insight into these size information, as well as for ease of comprehension, the HWHM size dependence on wavelength has been fitted by a power law of the form $q_{1/2}$ (l) = b × λ^a. The best fit values of '*a*' and '*b*' are listed in Table 6 for a few selected models. One typical example for each stellar type for uniform density case are also shown in Figure 6. The usefulness of the values of '*a*' & '*b*' are discussed in section 4.2.

Table 6. Fitted values of the parameters *a* & *b* of $\theta_{1/2}$ (λ) = *b* × λ^a

Spectral type	r^0		r^{-1}	
O4	τ_{100} = 0.040	τ_{100} = 0.26	τ_{100} = 0.040	τ_{100} = 0.26
	a = 0.54	*a* = 0.24	*a* = 0.12	*a* = 0.42
	b = 15.96	*b* = 16.02	*b* = 15.86	*b* = 15.48
O7	*a* = 0.69	*a* = 0.38	*a* = 0.14	*a* = 0.41
	b = 15.28	*b* = 15.45	*b* = 15.28	*b* = 14.93
*B*0.5	*a* = 0.99	*a* = 0.53	*a* = 0.16	*a* = 0.38
	b = 14.28	*b* = 14.82	*b* = 14.76	*b* = 14.45

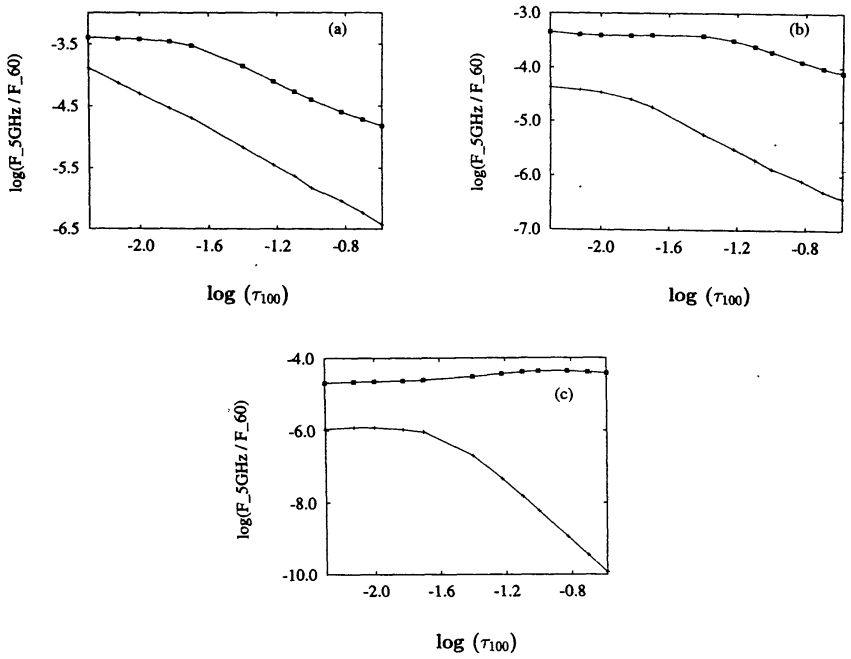

Figure 5. Plots of log of the ratio of radio flux density (F_{5GHz}) at 5GHz to the FIR flux density ($F_{60\ \mu m}$) at 60 μm as a function of the total radial optical depth (τ_{100}). The central stars in these models are : O4 in (a), O7 in (b) and B0.5 in (c). The symbols □ and + are for r^0 and r^{-1} density distributions respectively.

4. Discussion

With the aim of extracting some very basic and important parameters of compact H II regions, (viz., the type of the embedded star; the density and the temperature distribution in the cloud; the radial optical depth etc.), they have been modelled realistically and radiation transfer calculations were performed to predict their emergent SEDs, angular sizes etc. By exploring a realistic parameter space of several variables, it has been possible to identify those parts of the continuum SED, which play more significant role in deriving physical details of the compact HII regions. The model predictions when compared with observations, would quickly lead to conclusions regarding those parameters. This study is particularly a first step towards more detailed modelling of any target source by fine tuning the parameters further or introducing more details into the model. A more generalized study with fewer constraints and modelling of fine structure line emission from heavy elements in gas phase are presented in Mookerjea & Ghosh (1999, Paper II).

In order to have a conservative estimate of the colours, only those parts of the spectra are defined to be "measurable", where the emission from the cloud is substantially more than the contribution from the ISRF scattered by the outer regions of the cloud. As a result, the near infrared (< 3 μm) spectra are entirely unusable and between 5 & 10 μm, the spectral details are useful depending on the exciting star (O4 or O7 or B0.5).

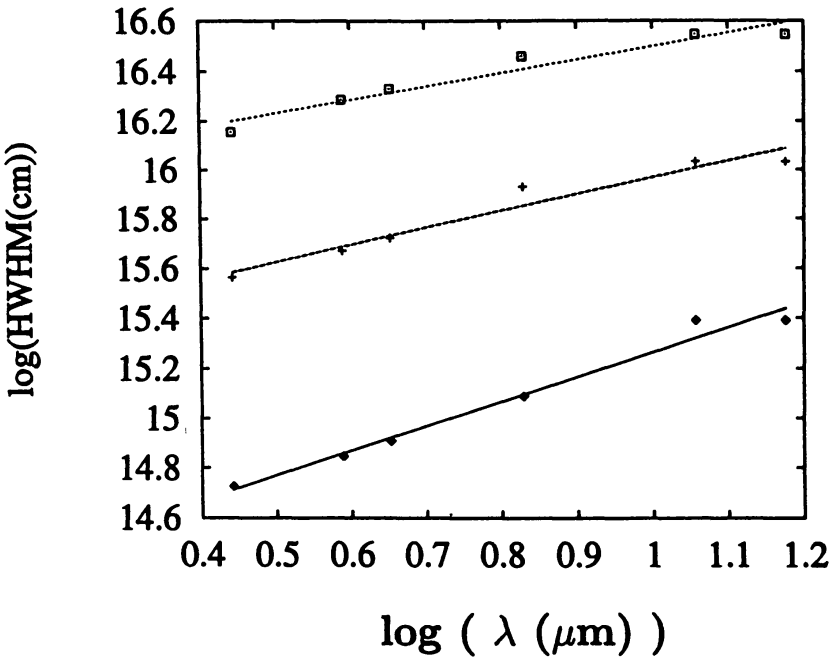

Figure 6. Plots of logarithms of half sizes (shown as points), as a function of logλ for τ_{100} = 0.040, with O4 (top curve), O7 (middle curve) and B0.5 (bottom curve) as central stars and uniform dust density distribution. The straight lines are the power law fits.

4.0.1. Mid infrared colours (PHT-P)

The mid-IR colour [P3-9] (Figure 2a) is measurable only if the exciting star is O4. For low or moderate optical depths ($\tau_{100} < 1$), this colour can easily distinguish the density distributions r^0 or r^{-1}. The spectrum is redder for r^{-1} than it is for r^0. The colour [P9-12] (Figures 2b, 3a) is measurable for O4 and O7 types. Once again the low and medium τ_{100} cases can distinguish the density distribution (redder for r^{-1}). On the other hand, the colour [P12-13] (Figures 2c, 3b, 4a) is measurable for all three types of exciting stars. At low optical depths ($\tau_{100} < 0.03$), although this colour cannot distinguish between the dust distributions, it is extremely sensitive to the type of the exciting star, hence can confirm the type as expected from total luminosity. If τ_{100} is greater than 0.1, then the dust density distribution law can be determined with ease. The colour [P13-14] (Figures 2d, 3c, 4b) again can easily unravel the dust density distribution, if the stellar type estimate is already available.

4.0.2 Far infrared colours (PHT-C)

The far-IR colour [C4-8] (Figures 2e, 3d, 4c), at higher optical depths ($\tau_{100} > 0.03$), can surprisingly confirm the type of the exciting star, though the colour measurement should be rather accurate (better than 0.05 dex). However, it is insensitive to the dust density distribution law except at the largest optical depths. At low τ_{100} the density distribution can be inferred provided this colour is known accurately. The colour [C8-11] (Figures 2f, 3e, 4d) is rather insensitive and demands even higher accuracy in measurement for extracting information. However, with modest accuracy, it can distinguish between a O4 and B0.5 star clearly. Inferring density distribution law needs about 0.02 dex accuracy.

4.1 Radio continuum to far infrared ratio

The radio continuum emission at 5 GHz has been computed from the transport calculations of stellar Lyman continuum photons through the gas and the dust and integrating the emission (without any assumption about the optical depth). The flux density at 60 μm is taken as a representative of far-IR emission. The ratio of radio continuum emission at 5 GHz and flux density at 60 μm ($F_{5GHz}/F_{60\mu m}$) are presented in Figure 7. This ratio is extremely sensitive to the density distribution as shown in Figure 7. Whereas for the O4 case, the ratio is very sensitive to τ_{100} for both the types of density distributions, for the other two cases (O7 and B0.5), only the r^{-1} density distribution is very sensitive to τ_{100} (above 0.01).

4.2 Structural information

The Table 6 quantifies sensitivity of the fitted parameters '*a*' and '*b*' to the (i) spectral type of embedded star, (ii) density distribution, & (iii) the optical depth. The following trends are noted. Whereas the overall angular size increases ('*b*' increases) as one goes from B0.5 to O7 to O4, the dependence on wavelength flattens ('*a*' reduces). This trend is very strong for the constant density case, irrespective of the optical depth. For the r^{-1} density distribution, whereas the dependence of '*b*' on spectral type of the star is seen clearly, the dependence of '*a*' becomes insensitive. However, in this case, '*a*' is still quite sensitive to the optical depth.

Hence, we conclude that if among the three primary details (viz., spectral type, density distribution & optical depth) of compact H II regions, any one of these is known, the other two can be reliably inferred from the spatial information.

5. Summary

The present study is aimed at identifying the wavelength regions, where the SED holds key information about the compact H II regions and quantifying their diagnostic values in terms of local slopes of the SEDs and dependence of the angular sizes on the wavelength. In addition, it presents approximate but quick conclusions about some basic parameters of compact H II regions, based on infrared photometric, imaging and / or spectroscopic measurements. This is of particular importance if the measurements are available for a large sample from a space mission like ISO. The idea being that of extracting crude first order parameters of compact H II regions before indulging into more sophisticated and detailed modelling of individual sources.

Self-consistent radiation transfer modelling have been carried out for the dust and the ionized as well as the neutral gas, for a large range of parameter space. Three types of exciting stars, ZAMS O4, O7 and B0.5, have been considered to be embedded at the centre of a spherical cloud with a radial density distribution given by a power law $n(r) \sim r^{-m}$; m = 0, 1. The following observables, viz., mid and far infrared photometric colours; angular sizes (HWHM) as a function of wavelength; and the radio continuum emission, have been predicted.

Since the total mass of the cloud for these models is assumed to be available through observations, the distance to the source must be known. Hence, the total luminosity and the physical size are also known. This implies that, for uniform density distribution, the total τ_{100} can be estimated and for r^{-1} an upper limit of τ_{100} may be derived. The observations need to be compared with a family of models covering a range of τ_{100} to arrive at the best description of the source.

The radio to far infrared ratio is a very good diagnostic for any spectral type of the embedded star, particularly for the r^{-1} density distribution law.

The structural information contained in radial profiles, as expressed at various wavelengths of ISOCAM filters, when parameterized by a best fit two parameter power law ($\theta_{1/2} \sim a \times \lambda^b$), also has a lot of diagnostic value.

The next step to the present study relaxes further the assumptions about the compact H II regions as well as includes a more sophisticated treatment of the gas component to predict fine structure line emission of heavy elements that are observable using the ISO spectrometers (Mookerjea & Ghosh, 1999, Paper II).

Acknowledgements

It is a pleasure to thank D. Narasimha for many useful discussions.

Appendix

A. Simple approach to radiative transfer through the gas

In this simple approach, the extent of the ionized region (in spherical geometry) is determined by transporting the Lyman continuum photons (from the centrally located star / star cluster) through the cloud including the effect of the dust, where they can exist (as determined by their sublimation). The gas component of the cloud is assumed to consist of only hydrogen. Next, the radio continuum emission emerging from the cloud is calculated by transporting the radio photons (free-free emission from the ionized medium of the cloud), through the entire cloud without making any approximation about the optical thinness of the gas (i.e self absorption is treated appropriately). The gas-dust coupling has been neglected.

A. 1. Extent of the ionized region

The size of the H II region has been calculated by considering photoionization and recombination of hydrogen, along with the absorption due to the dust grains. The presence of the dust component reduces the size of the ionized region, (R_{HII}), compared to that of pure gas Stromgren sphere considerably, depending on the density and the gas to dust ratio. The dust grains can exist in principle, only beyond a radial distance, say r_{subl}, depending on its sublimation temperature and the local radiation field. In practice, the actual distance beyond which the dust exists, say r_{fit}, is determined by the model fitting of the observed SED, by radiative transport calculations through the dust. The r_{fit} is often much larger than r_{subl}.

Hence, whether one encounters a dusty Stromgren sphere or not, is determined by the type of the star / integrated spectrum of the cluster; radial density distribution around the central star; and r_{fit}. We call it a Case A, if the ionized region extends into the region where the gas and the dust co-exist. The other case of entire ionized region devoid of any dust grains is termed Case B. So for Case B, the extent of the H II region can be obtained by solving the equation,

$$-dN(r) = 4\pi\alpha_2 r^2 n_e^2(r)dr \tag{A1}$$

where, N(r) is the Lyman continuum photon flux, α_2 is the recombination coefficient for hydrogen (for recombinations to all states except the ground state) and n_e is the number density of electrons or H^+ ions (for a pure H II region), which in our case is the gas number density (n_g) and may be given by,

$$n_g = n_0' \left(\frac{R_{min}}{r} \right)^m, \quad m= 0, 1, 2 \tag{A2}$$

For m = 0, 1, 2 equation (A1) can be solved easily by using the boundary condition

$$\text{at } r = r_*, \qquad N(0) = N_{Lyc} \tag{A3}$$

where, N_{Lyc} is the total number of Lyman continuum photons emitted per second by the embedded exciting star / star cluster and r_* is an effective stellar radius (with volume equal to the sum of that of all the stars of the embedded cluster; as it turns out, results are extremely insensitive to r_*).

In case A however, the ionizing (Lyman continuum) photons experience further attenuation due to direct absorption by the dust, so the modified radiation transfer equation would be,

$$- dN(r) = 4\pi r^2 \alpha_2 n_e^2 \, dr + N(r)\tau_{Lyc} \, dr \tag{A4}$$

where τ_{Lyc} refers to the optical depth of dust at $\lambda < 912$ Å. We solve the above equation, using the boundary conditions,

$$\text{at } r = R_{min} \qquad N(R_{min}) = N_1 \tag{A5}$$

where N_1 is determined by using equation (A1) and

$$\text{at } r = R_{HII} \qquad N(R_{HII}) = 0 \tag{A6}$$

A. 2. Calculation of continuum emission

With R_{HII} properly determined, the radio continuum emission which occurs due to the free-free emission from the ions and electrons can be calculated by using the formula (Spitzer 1978),

$$J_\nu = \int_{r*}^{R_{HII}} 4\pi r^2 (4\pi\varepsilon_\nu) \, e^{-\int_r^{R_{HII}} \kappa_\nu dr} \, dr \tag{A7}$$

where, the coefficients of emission ε_ν and absorption κ_ν are given by,

$$\varepsilon_\nu(\text{erg/cm}^3\text{/sec/sr/Hz}) = 5.44 \times 10^{-39} \, g_{ff} \, Z_i^2 \, n_e n_i T^{-0.5} e^{-h\nu/kT} \tag{A8}$$

$$\kappa_\nu(1/\mathrm{cm}) = 0.1731(1 + 0.130 \log(T^{3/2}\nu^{-1})Z_i^2 n_e n_i T^{-3/2}\nu^{-2} \quad \text{(A9)}$$

The Gaunt factor (g_{ff}), is given by,

$$g_{ff} = 9.77(1+ 0.130 \log (T^{3/2}\nu^{-1})) \quad \text{(A10)}$$

An electron temperature of 8000 K has been assumed for all calculations. The radio continuum has been calculated at a frequency of 5 GHz.

B. Numerical details regarding CSDUST3

We have used the code CSDUST3, with frequency and radial grids adequate for our problem, as described below.

B. 1. Frequency grid

The frequency grid consists of 89 points, ranging from 0.0944 to 5000 μm. Since, Draine & Lee (1984) give dust properties only upto 1000 μm, a power law extrapolation has been done beyond 1000 μm, upto 5000 μm. The frequency grid is not uniform and has been made finer within the wavebands of each of the ISOPHOT filters used in the present study.

B. 2. Radial grid

Essentially two types of radial grids have been used : one kind for the uniform (r^0) density distribution and another for the r^{-1} case. This was necessary because, the code CSDUST3 has convergence problems, if the distance between successive radial grid points is such that the optical depth ≈ 1 at any of the frequencies of the grid. This problem is most severe at the two boundaries of the cloud, where some UV radiation (stellar or ISRF) is incident, so that a finer grid is required there. Hence for the uniform density distribution, the entire radial range has been divided into two parts, with 71 points in a logarithmically increasing grid spacing in the first part (i.e., from the inner boundary to mid point of the cloud), and an exact mirror image on the second part. This gives a total of 141 radial grid points with a finer grid at both the boundaries. It may be noted, that the necessity for having a fine grid towards the outer boundary of the cloud, exists only for uniform density distribuion, since in this case alone there remains enough dust grains to produce high optical depth at the outer boundary. For the case of r^{-1} density distribution, the dust density falls off so rapidly, that towards the outer edge, the optical depth between successive radial grid points is never large enough. As a result, a smooth convergence is achieved even with a logarithmically increasing grid spacing right from the inner to the outer boundary of the cloud.

References

Cesarsky C. J. et al. 1996, ApJ, 315, L32.

Draine B. T., Lee H. M., 1984, ApJ, 285, 89.

Egan M. P., Leung C. M., Spagna G. F., 1988, Computer Physics Communications, 48, 271.

Ferland G. J., Hazy a Brief Introduction to CLOUDY, Univ. of Kentucky, Dept. of Phys. and Astron. Internal

Reports, 1996.

Kessler M. F. et al., 1996, A&A, 315, L27.

Klaas U., Kruger H., Heinrichsen I., Heske A., Laureijs R., ISOPHOT Observer's Manual, pages 12 & 14, 1994.

Laor A., Draine B. T., 1993, ApJ, 402, 441.

Lemke D. et al., 1996, A&A, 315, L64.

Mathis J. S., Mezger P. G., Panagia N., 1983, A&A, 128, 212.

Mathis J. S., Rumpl W., Nordsieck K. H., 1977, ApJ, 217, 425.

Mookerjea B., Ghosh S. K., Karnik A. D., Rengarajan T. N., Tandon S. N., Verma R. P., 1999, ApJ, 522, 285.

Mookerjea B., Ghosh S. K., 1999, J. Astrophys. Astr., 20, in press.

Mookerjea B., Ghosh S. K., 1999, BASI (Paper II), 27, 601.

Panagia N., 1973, AJ, 78, 9.

Puget J. L. & Leger A. 1989, ARA&A, 27, 161.

Spitzer L., Physical Processes in the Interstellar Medium, 1978.

Thompson R. I., 1984, ApJ, 283, 165.